Nonlinear coupling mechanism in a quantum system

Jing-Dong Bao
Department of Physics, Beijing Normal University, Beijing 100875, China
(Received 6 September 2001; revised manuscript received 10 December 2001; published 8 May 2002)

For a quantum system coupled to a heat bath environment the nonlinear dissipation is studied starting from imaginary-time path-integral formulation. An effective classical potential (ECP) is obtained in which not only the frequency of the potential but also the slope of the coupling form factor are treated as trial functions, they are determined by minimizing the effective classical potential. Further, terms of higher order are also added in an improved Gaussian measure in order to regularize integrals of fluctuation modes at low temperatures. Various approximations to thermodynamic functions of a double-well potential are compared with the dissipative path-integral Monte Carlo method. In particular, it occurs for single- or double-well potentials, where nonlinear dissipation can induce the appearance of multistable states and barrier drift. Nonmonotonic varying of the barrier height of the ECP with temperature is found in a bistable system.

DOI: 10.1103/PhysRevA.65.052120 PACS number(s): 03.65.Yz, 03.65.Db, 05.70.Ce

I. INTRODUCTION AND MODEL

The system-plus-reservoir model is the most common approach to the treatment of quantum dissipation. This model considers the dissipation in a system to be due to the interaction with a reservoir consisting of a continuum of harmonic oscillators [1–5], and the latter is at thermal equilibrium [6]. By means of the imaginary-time path-integral technique it is possible to integrate out the bath variables and then to produce a nonlocal influence action. Usually, one assumes that the coupling between the system and reservoir is bilinear in the system and bath coordinates. This is called a linear or homogeneous dissipation mechanism, where the friction is equal to a constant.

Dependence of the coupling form factor on the system coordinate is often used in the modeling of charge-transfer reactions, in which a nonlinear solute dipole moment function changes as a function of the reaction coordinate and is coupled to a local solvent-generated electric field exhibiting Gaussian fluctuation [7]. In fact, friction of a system near the well and that near the barrier may be quite different from each other, it has been shown that the introduction of coordinate-dependent friction can lead to qualitatively different physics [8]. For nuclear fission and fusion dynamics, the friction depends strongly on the collective coordinates, for instance, the friction along the center-of-mass distance of two fragments varies and reaches a maximum at the scission point and then vanishes [9]. Indeed, the dynamics near a potential barrier plays an important role in almost all areas of physics and chemistry [10,11]. In the quantum regime, the height, the position, and the curvature of hindered barrier should have a large deviation from the static potential in the presence of a nonlinear dissipative environment.

The Lagrangian of the whole system under study reads

$$L=\frac{1}{2}M\dot{x}^2-V(x)+\frac{1}{2}\sum_{\alpha=1}^{N} m_\alpha\left\{\dot{q}_\alpha^2-\omega_\alpha^2\left[q_\alpha-\frac{c_\alpha}{m_\alpha\omega_\alpha^2}f(x)\right]^2\right\}. \quad (1)$$

Here the coupling term is written in a form that does not lead to a coupling induced renormalization of the potential. The dependence of the classical friction on the system-coordinate arises from the nonlinear form factor $f(x)$, namely, the system coordinate-dependent classical friction in this model is given by

$$\gamma_{cl}(t;x)=\sum_{\alpha=1}^{N}\frac{f'(x)^2}{m_\alpha\omega_\alpha^2}\cos\omega_\alpha t, \quad (2)$$

where $f'(x)$ is the derivative of the function $f(x)$ with respect to x. For the case where the derivative $f'(x)$ is independent of x and equal to a constant, the resulting "linear" dissipation is characterized by a spectral density $J(\omega)$ such that the classical friction kernel is given by

$$\gamma_{cl}(t)=\frac{2}{\pi}\int_0^\infty d\omega\frac{J(\omega)}{\omega}\cos\omega t. \quad (3)$$

Previous works for the coordinate-dependent friction attached importance to the classical cases. In the present study, large nonlinear coupling effects are shown to form a picture of the proposed effective classical potential (ECP) in the quantum regime. To this end, we choose to periodically continue paths $x(\tau)$ and $q_\alpha(\tau)$ in the imaginary time $\tau=it$,

$$\{x(\tau),f(x(\tau)),q_\alpha(\tau)\}=\sum_{n=-\infty}^{\infty}\{X_n,f_n,q_{\alpha,n}\}\exp(i\theta_n\tau), \quad (4)$$

where $X_n=X_{-n}^*$, $f_n=f_{-n}^*$, $q_{\alpha,n}=q_{\alpha,-n}^*$, and $\theta_n=2\pi n/(\hbar\beta)$ are the Matsubara frequencies. By integrating out the environment degrees of freedom, for an open quantum system it is still convenient to work with the path-integral representation of the reduced partition function,

$$Z=\int_{-\infty}^{\infty}\frac{dX_0}{\sqrt{2\pi\hbar^2\beta/M}}\int\mathcal{D}[x_1(\tau)]\exp\{-S_{eff}^E[x(\tau)]/\hbar\}, \quad (5)$$

where the functional measure is written as

$$\int \mathcal{D}[x_1(\tau)] = \prod_{n=1}^{\infty} \left[\int_{-\infty}^{\infty} \int_{-\infty}^{\infty} \frac{d\,\mathrm{Re}\,X_n d\,\mathrm{Im}\,X_n}{\pi/(M\beta\theta_n^2)} \right], \quad (6)$$

and the effective Euclidean action is given by

$$S_{eff}^{E}[x(\tau)] = \int_0^{\hbar\beta} d\tau \left[\frac{1}{2} M\dot{x}^2 + V(x(\tau)) \right] + \frac{1}{2} \int_0^{\hbar\beta} d\tau \int_0^{\hbar\beta} d\tau' k(\tau-\tau') f(x(\tau)) f(x(\tau')), \quad (7)$$

with the influence kernel $k(\tau)$,

$$k(\tau-\tau') = \sum_{\alpha=1}^{N} \left(\frac{c_\alpha^2}{m_\alpha \omega_\alpha^2} : \delta(\tau-\tau') : - \frac{c_\alpha^2}{2 m_\alpha \omega_\alpha} \frac{\cosh[\omega_\alpha(\hbar\beta/2 - |\tau-\tau'|)]}{\sinh(\omega_\alpha \hbar\beta/2)} \right), \quad (8)$$

where $:\delta(\tau-\tau'):$ is a generalized δ function with period $\hbar\beta$.

The quantum statistical properties of an equilibrium system or the decay rate of a metastable state can be computed directly if the partition function is known. Unfortunately, the path sum can be performed exactly only when the action is a quadratic form in the system coordinate. For a conservative system, the effective classical partition function has been evaluated by the variational perturbation path-integral approach [12–14]. However, only a little work generalized this approach to linear [5,15,16] and nonlinear [17,18] dissipative systems. It is, therefore, important to work out an optimal produce by improving the Gaussian measure including the nonlinear dissipative part of the action.

The rest of this paper is organized as follows. In Sec. II a second-order effective classical potential is obtained first in which we introduce two trial parameters such as the frequency of potential and the slope of the coupling function; further, an important Gaussian measure is proposed in order to regularize the divergent integrals of the dangerous modes of second order. Some applications are addressed in Sec. III, various approximations to thermodynamic functions of a double-well potential are compared with the dissipative path-integral Monte Carlo method (DPIMC) [19–21]. Indeed, it is observed that nonlinear coupling can induce the appearance of multistable states in a harmonic potential; moreover, nonmonotonic behavior of the temperature-dependent barrier height of the ECP of a double-well potential is found and analyzed. Finally, Sec. IV offers some conclusions.

II. EFFECTIVE CLASSICAL POTENTIAL

A. Second-order Gaussian measure

To perform the analytical integrals over all Fourier components of environment variables in Eq. (5), the reduced partition function can be rewritten in a classical form with an ECP $W(x_0)$, i.e.,

$$Z = \int_{-\infty}^{\infty} [M/(2\pi\hbar^2\beta)]^{1/2} dx_0 \exp[-\beta W(x_0)], \quad (9)$$

here $x_0 = (\hbar\beta)^{-1} \int_0^{\hbar\beta} x(\tau) d\tau$ is the centroid of the thermal path [22].

To find an approximation to $W(x_0)$, we decompose the potential and coupling function as follows:

$$V(x(\tau)) = \frac{1}{2} M\Omega^2(x_0)[x(\tau)-x_0]^2 + \tilde{V}(x(\tau)),$$

$$f(x(\tau)) = \mu(x_0)[x(\tau)-x_0] + \tilde{f}(x(\tau)); \quad (10)$$

also the influence kernel is represented as a Fourier series

$$k(\tau) = (\hbar\beta)^{-1} \sum_{n=-\infty}^{\infty} K(\theta_n) \exp(i\theta_n \tau) \quad (11)$$

with

$$K(\theta_n) = \sum_{\alpha=1}^{N} \frac{c_\alpha^2}{m_\alpha \omega_\alpha^2} \frac{\theta_n^2}{(\theta_n^2 + \omega_\alpha^2)}. \quad (12)$$

Substituting Eqs. (4), (10), and (11) into the partition function (5), we evaluate exactly the integrals over the quadratic part of the fluctuation modes of the system coordinate,

$$\exp[-\beta W(x_0)] = Z_1(x_0) \left\langle \exp\left\{ -\frac{1}{\hbar} \int_0^{\hbar\beta} d\tau \tilde{V}(x(\tau)) - \frac{1}{2\hbar} \int_0^{\hbar\beta} d\tau \int_0^{\hbar\beta} d\tau' k(\tau-\tau') \times \tilde{f}(x(\tau)) \tilde{f}(x(\tau')) \right\} \right\rangle_1, \quad (13)$$

where $\langle \cdots \rangle_1$ denotes the expecting value calculated by the following Gaussian distribution:

$$Z_1^{-1}(x_0) \exp\left(-M\beta \sum_{n=1}^{\infty} A_n |X_n|^2 \right) \quad (14)$$

with

$$A_n = \theta_n^2 + \Omega^2(x_0) + \frac{K(\theta_n)\mu^2(x_0)}{M} \quad (15)$$

and

$$Z_1=\prod_{n=1}^{\infty}\theta_n^2[\theta_n^2+\Omega^2(x_0)+\mu^2(x_0)K(\theta_n)/M]^{-1}. \quad (16)$$

Applying the Jensen-Peierls inequality $\langle e^{-\mathcal{F}}\rangle \geqslant e^{-\langle\mathcal{F}\rangle}$ to Eq. (13), we give an upperbound $W_1(x_0)$ for $W(x_0)$,

$$W_1(x_0)=\frac{1}{\beta}\sum_{n=1}^{\infty}\ln(A_n\theta_n^{-2})+V_{a^2}(x_0)-\frac{1}{2}M\Omega^2(x_0)a^2(x_0)+\frac{1}{2\hbar\beta}\int_0^{\hbar\beta}d\tau\int_0^{\hbar\beta}d\tau' k(\tau-\tau')\times\langle f(x(\tau))f(x(\tau'))\rangle_1-\frac{1}{M\beta}\sum_{n=1}^{\infty}\frac{K(\theta_n)\mu^2(x_0)}{A_n}, \quad (17)$$

where $V_{a^2}(x_0)$ and $\langle f(x(\tau))f(x(\tau'))\rangle_1$ arise from smearing them out in the neighborhood of each point x_0 with the distribution (14) [13,17,23],

$$\langle V(x(\tau))\rangle_1=\int_{-\infty}^{\infty}\frac{dx}{\sqrt{2\pi a^2}}V(x)\exp\left[-\frac{(x-x_0)^2}{2a^2}\right] \quad (18)$$

and

$$\langle f(x(\tau))f(x(\tau'))\rangle_1=\frac{1}{2\pi\sqrt{a^4-b^4}}\int_{-\infty}^{\infty}\int_{-\infty}^{\infty}dx_1dx_2f(x_1)f(x_2)\times\exp\left[-\frac{(x_1+x_2-2x_0)^2}{4(a^2+b^2)}-\frac{(x_1-x_2)^2}{4(a^2-b^2)}\right] \quad (19)$$

with

$$b^2(x_0,\tau-\tau')=2(M\beta)^{-1}\sum_{n=1}^{\infty}\cos[\theta_n(\tau-\tau')]A_n^{-1} \quad (20)$$

and $a^2(x_0)=b^2(x_0,0)$.

We are in a position to determine the two unknown x_0-dependent trial functions $\Omega^2(x_0)$ and $\mu^2(x_0)$ by minimizing $W_1(x_0)$, i.e.,

$$(W_1')_{\Omega^2}=\frac{\partial W_1}{\partial\Omega^2}+\frac{\partial W_1}{\partial a^2}\frac{\partial a^2}{\partial\Omega^2}+\frac{\partial W_1}{\partial b^2}\frac{\partial b^2}{\partial\Omega^2}=0,$$

$$(W_1')_{\mu^2}=\frac{\partial W_1}{\partial\mu^2}+\frac{\partial W_1}{\partial a^2}\frac{\partial a^2}{\partial\mu^2}+\frac{\partial W_1}{\partial b^2}\frac{\partial b^2}{\partial\mu^2}=0. \quad (21)$$

The solutions of the optimal $\Omega^2(x_0)$ and $\mu^2(x_0)$ are given by

$$\Omega^2(x_0)=\frac{2}{M}\left\{\frac{\partial V_{a^2}}{\partial a^2}+\frac{1}{2\Delta}\sum_{l=1}^{\infty}\sum_{n=1}^{\infty}\times\frac{[K^2(\theta_l)-K(\theta_l)K(\theta_n)]I_n}{A_l^2A_n^2}\right\} \quad (22)$$

and

$$\mu^2(x_0)=\frac{1}{\Delta}\sum_{l=1}^{\infty}\sum_{n=1}^{\infty}\frac{[K(\theta_l)-K(\theta_n)]I_l}{A_l^2A_n^2}, \quad (23)$$

where

$$\Delta=\sum_{l=1}^{\infty}\sum_{n=1}^{\infty}\frac{K^2(\theta_l)-K(\theta_l)K(\theta_n)}{A_l^2A_n^2} \quad (24)$$

and

$$I_n=(\hbar\beta)^{-1}\int_0^{\hbar\beta}d\tau\int_0^{\hbar\beta}d\tau' k(\tau-\tau')\times\left\{\frac{\partial}{\partial a^2}\langle f(x(\tau))f(x(\tau'))\rangle_1+\cos\theta_n(\tau-\tau')\times\frac{\partial}{\partial b^2}\langle f(x(\tau))f(x(\tau'))\rangle_1\right\}. \quad (25)$$

The self-consistent equations (20)–(25) must be solved numerically at each point x_0 by iteration.

B. Important Gaussian measure

When temperature decreases and approaches to the crossover temperature T_c determined from $A_1(T_c)=0$ at the well-potential top [3–5], we improve the Gaussian measure (14) and make the trial action contain as much information as possible. Because the influence action in Eq. (7) is entirely *nonlocal*, $f(x)$ needs particularly to be expanded to the second-order at low temperatures. We split the action into three parts after decomposing the potential and coupling function as

$$V(x(\tau))=\frac{1}{2}M\Omega^2(x_0)[x(\tau)-x_0]^2+\frac{1}{4}Mc_4[x(\tau)-x_0]^4+\tilde{V}(x(\tau)),$$

$$f(x(\tau))=\mu(x_0)[x(\tau)-x_0]+\frac{1}{2}\lambda(x_0)[x(\tau)-x_0]^2+\tilde{f}(x(\tau)), \quad (26)$$

so that

$$S_{eff}^E=S_{qua}^E+S_{hig}^E+S_{rem}^E. \quad (27)$$

In Eq. (27) the first term is the quadratic part of the action,

$$S^E_{qua}=M\hbar\beta\sum_{n=1}^{\infty}A_n|X_n|^2, \tag{28}$$

the second term is a part of the fourth-order and cross amplitudes,

$$S^E_{hig}=\frac{3}{4}M\hbar\beta\sum_{n=-\infty}^{\infty}\left\{\left[c_4(x_0)+\frac{1}{2}\lambda^2(x_0)M^{-1}K(2\theta_n)\right]X_n^2X_{-n}^2+2\mu(x_0)\lambda(x_0)M^{-1}K(\theta_n)X_0X_nX_{-n}\right\}, \tag{29}$$

and the third term describes all remaining terms,

$$S^E_{rem}=\int_0^{\hbar\beta}\left[V(x(\tau))-\frac{1}{2}M\Omega^2(x_0)(x(\tau)-x_0)^2\right]d\tau+\frac{1}{2}\int_0^{\hbar\beta}d\tau\int_0^{\hbar\beta}d\tau' k(\tau-\tau')\{f(x(\tau))f(x(\tau'))-\mu^2(x_0)[x(\tau)-x_0][x(\tau')-x_0]\}-S^E_{hig}. \tag{30}$$

Substituting Eqs. (26) and (27) into Eq. (5) and performing the integrals over the fluctuation modes of the system coordinate, we have

$$\begin{aligned}\exp[-\beta W_2(x_0)]&=\int D[x_1(\tau)]\exp\left[-M\beta\sum_{n=1}^{\infty}\Lambda_n|X_n|^2\right]\times\exp\left\{-M\beta\sum_{n=1}^{\infty}(A_n-\Lambda_n)|X_n|^2-\frac{1}{\hbar}(S^E_{hig}+S^E_{rem})\right\}\\&=Z_2(x_0)\left\langle\exp\left[-M\beta\sum_{n=1}^{\infty}(A_n-\Lambda_n)|X_n|^2-\frac{1}{\hbar}(S^E_{hig}+S^E_{rem})\right]\right\rangle_2,\end{aligned} \tag{31}$$

where $\langle\cdots\rangle_2$ denotes the expectation value calculated by an improved Gaussian probability distribution

$$Z_2^{-1}(x_0)\exp\left(-M\beta\sum_{n=1}^{\infty}\Lambda_n|X_n|^2\right) \tag{32}$$

with $Z_2(x_0)=\Pi_{n=1}^{\infty}\theta_n^2\Lambda_n^{-1}$. Note that Λ_n is an effective eigenvalue, which consists of the contribution of higher orders, Eq. (29), and is evaluated similar to Refs. [3–5] as

$$\Lambda_n=\sqrt{\frac{2B}{\pi M\beta}}\,\mathrm{erfc}^{-1}[A_n'(M\beta/2B)^{1/2}]\exp[-(A_n')^2M\beta/2B], \tag{33}$$

where

$$B=3c_4(x_0)+\frac{3}{2}\lambda^2(x_0)M^{-1}K(\theta_{2n}),$$

$$A_n'=A_n+3x_0\mu(x_0)\lambda(x_0)M^{-1}K(\theta_n). \tag{34}$$

Applying the Jensen-Peierls inequality to Eq. (31), we obtain a more accurate approximation $W_2(x_0)$ to $W(x_0)$, i.e.,

$$\begin{aligned}W_2(x_0)=&\frac{1}{\beta}\sum_{n=1}^{\infty}\ln(\Lambda_n\theta_n^{-2})+\frac{2}{\beta}\sum_{n=1}^{\infty}(A_n-\Lambda_n)/\Lambda_n\\&+V_{a^2}(x_0)-\frac{1}{2}M\Omega^2(x_0)a^2(x_0)\\&+\frac{1}{2\hbar\beta}\int_0^{\hbar\beta}d\tau\int_0^{\hbar\beta}d\tau' k(\tau-\tau')\\&\times\langle f(x(\tau))f(x(\tau'))\rangle_2\\&-\frac{1}{M\beta}\mu^2(x_0)\sum_{n=1}^{\infty}K(\theta_n)\Lambda_n^{-1},\end{aligned} \tag{35}$$

where $V_{a^2}(x_0)$ and $\langle f(x(\tau))f(x(\tau'))\rangle_2$ arise from smearing them out in the neighborhood of each point x_0 with the distribution (32), and

$$b^2(x_0,\tau-\tau')=2(M\beta)^{-1}\sum_{n=1}^{\infty}\cos[\theta_n(\tau-\tau')]\Lambda_n^{-1} \tag{36}$$

and $a^2(x_0)=b^2(x_0,0)$.

Clearly, $\Lambda_n>A_n$, the second term on the right-hand side of Eq. (35) is always negative, this may lead to a better result $W_2(x_0)<W_1(x_0)$ at each point, moreover, Λ_n^{-1} remains finite when $T\to T_c$ and $\Lambda_n\to A_n'$ when $T\gg T_c$. Here, only Λ_1 is used instead of A_1' and $\Lambda_n=A_n'$ $(n\geqslant 2)$. Equation (35) involves the four unknown x_0-dependent functions $\Omega^2(x_0)$, $c_4(x_0)$, $\mu(x_0)$, and $\lambda(x_0)$, they can be determined by minimizing $W_2(x_0)$. Here we consider only the solutions of equations: $(W_2')_{\Omega^2,\mu^2}=0$ [17], while the higher-order coefficients $c_4(x_0)$ and $\lambda(x_0)$ are taken to be two adjustable parameters for giving the best minimum of $W_2(x_0)$ at each thermal centroid x_0.

III. APPLICATION

A. Thermodynamic functions

The typical thermodynamic functions such as the free energy F, the inertial energy U, and the entropy S are determined by

$$F=-\beta^{-1}\ln Z,\quad U=-\frac{\partial}{\partial\beta}\ln Z,\quad S=\beta(U-F). \tag{37}$$

A Drude model with real-time memory damping is chosen,

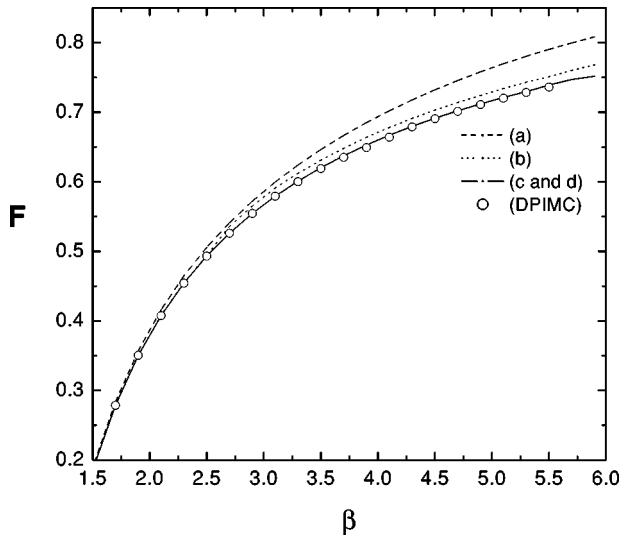

FIG. 1. The calculated free energy as a function of the inverse temperature. See text for details.

$$\gamma(t)=\frac{\gamma_0}{\tau_D}\exp\left(-\frac{t}{\tau_D}\right), \tag{38}$$

where γ_0 is the zero-frequency damping constant and τ_D is the memory time, thus $J(\omega)=M\gamma_0\omega/[1+(\omega\tau_D)^2]$.

In this paper, we use natural units with $\hbar=M=1$. In Figs. 1–3, various approximations are applied to calculate the above three quantities as functions of the inverse temperature β, and they are compared with the DPIMC [20,21] results. Here we consider a double-well potential

$$V(x)=V_1(x)=-\frac{1}{2}x^2+\frac{1}{4}x^4 \tag{39}$$

and a corrected linear coupling function [7,24]

$$f(x)=f_1(x)=x\{1+\epsilon[1-\exp(-hx^2)]\}. \tag{40}$$

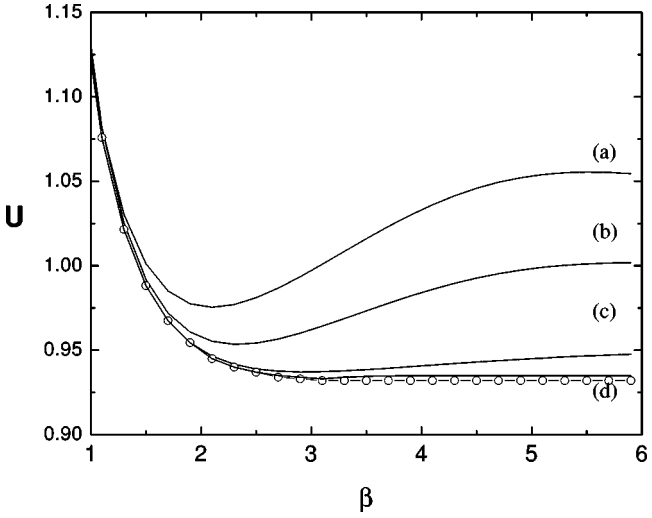

FIG. 2. The calculated inertial energy as a function of the inverse temperature. See text for details.

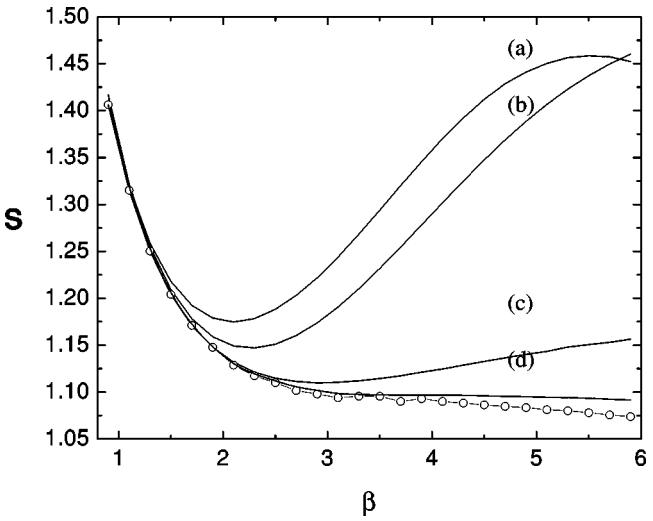

FIG. 3. The calculated entropy as a function of the inverse temperature. See text for details.

The parameters used are $\epsilon=0.5$, $h=1.0$, $\gamma_0=1.0$, and $\tau_D=4.0$.

In these figures the lines from top to bottom are the results evaluated, respectively, by (a) the F-K method of the conservation system [$c_4=\mu=\lambda=0$] [13,14]; (b) the local linear approximation to the coupling function [$c_4=0$, $\mu(x_0)=f_1'(x_0)$, $\lambda=0$], (c) the second-order Gaussian measure method [$c_4=\lambda=0$] [17], and (d) the improved Gaussian measure method. The open circles are the DPIMC data. It is readily seen that the present approach (d) gives the lowest limits for these quantities. The calculated results of the free energy by using the methods (c) and (d) are identical, as can be verified visually. Nevertheless, the numerical error for the internal energy and the entropy increases when the temperature decreases. Our approximation is quite reliable up to $\beta=5$. When T decreases and approaches the crossover temperature T_c, the eigenvalues of the fluctuation modes X_1 and X_{-1} are very small, thus the integrals over amplitudes X_1, X_{-1} become divergent in the methods (a)–(c). This problem has been regularized by adding partial fourth-order terms in the trial function. Approximation (d) may be improved further by using the third-order perturbation [25,26] under the present important Gaussian distribution (32).

B. ECP of single-well potential

We calculate now the ECP of a harmonic potential V_2 in the presence of an inhomogeneous coupling f_2 [2], i.e.,

$$V(x)=V_2(x)=\frac{1}{2}x^2 \tag{41}$$

and

$$f(x)=f_2(x)=\exp[-(x-x_b)^2/\sigma]. \tag{42}$$

In Figs. 4(a) and 4(b), the ECP $W_2(x_0)$ is plotted for various temperatures and damping constants. The common parameters used are $\tau_D=0.25$, $\sigma=0.2$, and $x_b=0$. The ef-

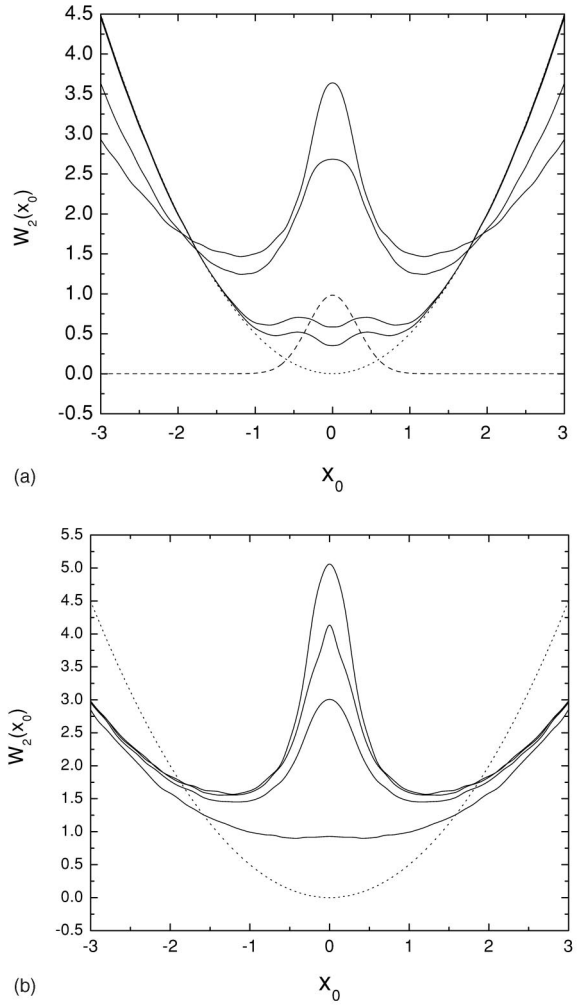

FIG. 4. The effective classical potential (solid lines) of the harmonic potential. The dotted line is $V_2(x_0)$, the dashed line is $f_2(x_0)$. (a) $W_2(x_0)$ at fixed $\gamma_0=4.0$ and for various temperatures $T=0.2$, 0.4, 2.0, and 3.0 from top to bottom; (b) $W_2(x_0)$ at fixed $T=0.3$ and for various damping constants $\gamma_0=8.0$, 6.0, 3.0, and 0.5 from top to bottom.

fects of nonlinear quantum dissipation have been shown in the shapes of ECP. Two observations can be made: First, quantum effects give rise to a temperature-dependent effective classical potential. Second, the position-dependent coupling induces the appearance of multistable states. Moreover, the energy difference between the grown barrier and the new ground states increases when the temperature decreases, this is opposite to the phenomena of quantum fluctuation wiping out a double-well potential in the absence of dissipation [13,14] or in the presence of a linear dissipation [5].

As a consequence of Eq. (33), the higher-order coefficients c_4 and $\lambda(x_0)$ play important roles in the improved Gaussian measure at low temperatures, when the temperature increases, Λ_n approaches A_n' (near $x_0=0$, $\mu\simeq 0$, thus $\Lambda_n \simeq A_n$). The influence of the derivation $\mu(x_0)$ of $f_2(x)$ on $W_2(x_0)$ is observably at moderate-to-larger temperatures. The curvature of $f_2(x_0)$ takes a maximum value and its slope equals zero at the minimum ($x_0=0$) of $V_2(x_0)$, hence the ECP is raised around the original point of the coordinate, and the nonlocal variance (proportional to the damping constant) of f_2 increases the effective action and $W_2(x_0=0)$ at low temperatures. Moreover, the maximum value of the derivation of $f_2(x)$ is determined by $f_2''(x)|_{x=x_m}=0$, i.e., $x_m=\pm\sqrt{\sigma/2}$; one can see a pair of local maxima of $W_2(x_0)$ (i.e., two additional unstable points) appear near x_m at moderate temperatures.

Starting from a viewpoint of quantum fluctuation, the above phenomenon is also understood well. Around the minimum of $V_2(x_0)$, the quantum fluctuation helps the particle to arrive at a position with high potential energy at low temperatures. Since the curvature of f_2 is maximum at the minimum of the potential, the contribution of f_2 raises the top of the ECP barrier when temperature decreases. On the other hand, the quantum fluctuation enhances the width of the harmonic potential; when the thermal centroid x_0 departs from the original point, the contribution of the influence action of f_2 to the ECP decreases and eventually vanishes, leading to a decrease in the ECP, so that the double stable states occur. At moderate-to-large temperatures, quantum fluctuation becomes weak and then the value of the influence action near $x_0=0$ is small, thus dissipation will not lead to an observable increasing of the ECP at the minimum of the potential. However, around the point x_m, where the slope of $f_2(x)$ is large and, thus, a strong friction raises the ECP, a local barrier, therefore, appears.

C. ECP of double-well potential

In the classical cases, the generalized Langevin equation for the system coordinate usually provides an adequate description of the barrier dynamics. Now, we study the finite temperature regime where the nonlinear quantum dissipation leads to a large deviation of the barrier from the classical one, when the couplings between the system and environment are different at the barrier top and at the well minimum. A simple symmetrical double-well potential is

$$V(x)=V_3(x)=-2x^2+x^4 \tag{43}$$

and another form of the coupling form factor [27] is

$$f(x)=f_3(x)=\tanh[\lambda(x-x_b)]. \tag{44}$$

In Figs. 5 and 6, the ECPs are plotted for f_2 and f_3 couplings at different temperatures. When the temperatures approach to T_c, both anharmonicities of the potential barrier and the nonlinearity of the coupling are always essential. The competition between the quantum fluctuation decreasing the ECP and the nonlocal dissipation increasing the ECP leads to the top of the ECP barrier rising as a nonmonotonic function of temperature.

In Fig. 7, we consider that the maximum of curvature of the coupling function is not at the classical potential barrier ($x_b\neq 0$). The result shows that the original symmetrical double-well potential is changed into an asymmetrical metastable potential, and the ECP barrier drifts toward the peak of f_2, where the nonlocal dissipation is the strongest.

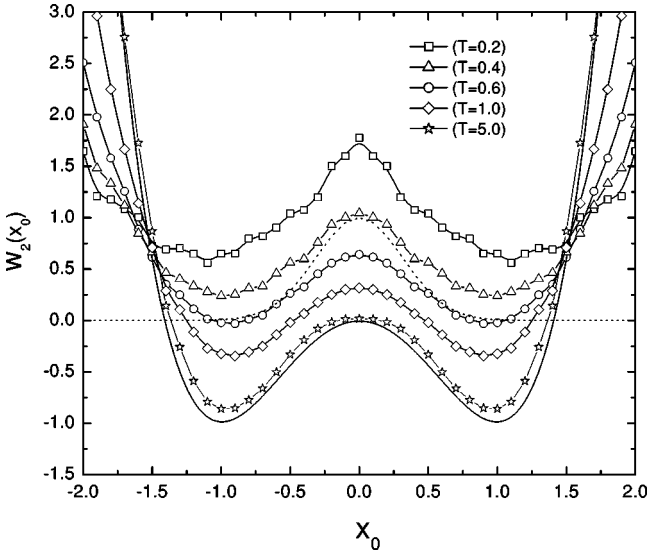

FIG. 5. The effective classical potential of the double-well potential in the presence of f_2 coupling for various temperatures. The solid line is $V_3(x_0)$ and the dotted line is $f_2(x_0)$.

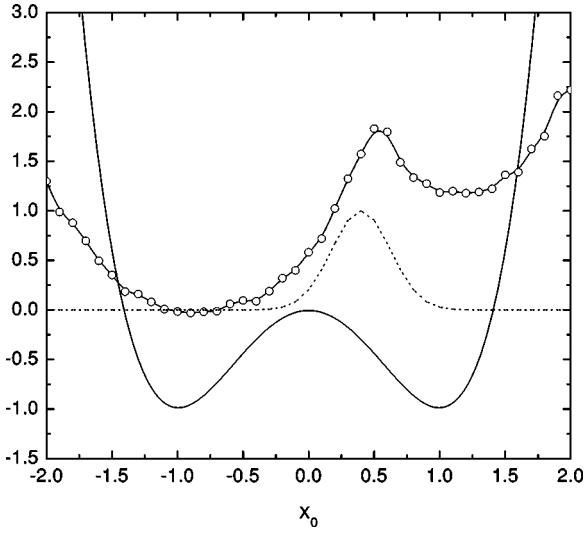

FIG. 7. The ECP of V_3 in the presence of f_2 coupling (dotted line) with the parameters $\gamma_0=4.0$, $\tau_D=0.5$, $x_b=0.4$, $\sigma=0.1$, and $T=0.2$. The solid line is $V_3(x_0)$ and the open circles indicate $W_2(x_0)$.

The barrier height $\Delta W_2(x_0)$ of the ECP is shown as a function of temperature in Fig. 8 for different coupling mechanisms. A nonmonotonic behavior of the barrier is observed in the presence of a nonlinear coupling. Because the dissipations are different at the static barrier and at the minima of the double-well potential, the ECP is risen inhomogeneously. At moderate-to-large temperatures, the f_3 coupling induced arising of the ECP at the top of the potential is larger than at the minimum of $V_3(x)$, thus the barrier height of the ECP is larger than the classical one. However, for f_2 coupling, the dissipation at the top of the ECP barrier is weak, and the quantum fluctuation gives rise to the potential, so the barrier height of the ECP in the presence of f_2 coupling is less than the classical one.

IV. CONCLUSIONS

The description of nonlinear coupling between the system and the reservoir within the framework of the imaginary-time functional representation has been discussed in the literature. A variational path-integral technique is applied to an inhomogeneous dissipative system, and then an effective classical potential is obtained. For a double-well potential, the present improved Gaussian measure approach gives more accurate results for the thermodynamic functions, i.e., the lowest limits of these quantities. Further, the integrals over the dangerous modes have been regularized when the temperature decreases and approaches the crossover temperature. It is also demonstrated that the nonlinearity of the coupling function plays an important role in the effective classical potential.

For a quantum system in the absence of dissipation or in the presence of linear dissipation, the ECP barrier of a

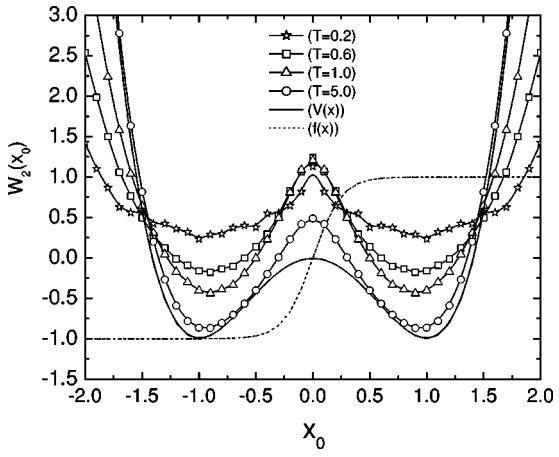

FIG. 6. The effective classical potential of the double-well potential in the presence of f_3 coupling for various temperatures. The solid line is $V_3(x_0)$ and the dotted line is $f_3(x_0)$.

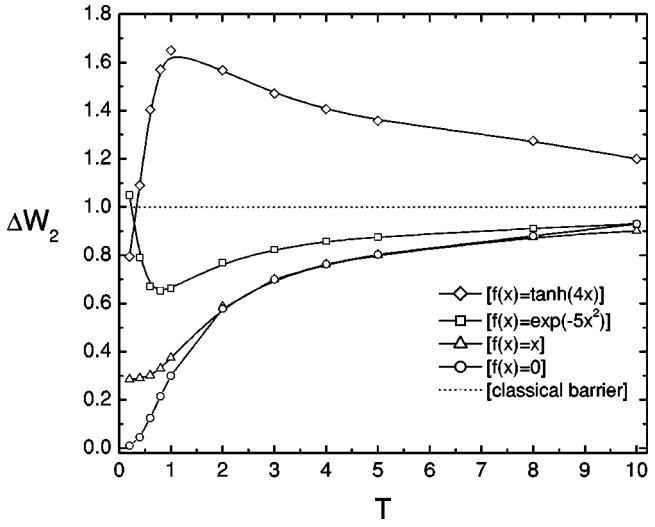

FIG. 8. Dependence of the barrier height of ECP of the double-well potential V_3 on temperature for different coupling mechanisms.

double-well potential is eliminated, and the ECP width of a single-well potential is enhanced only. However, in the presence of an inhomogeneous dissipation, the present results show that cooperation and competition between quantum fluctuation and dissipation can induce the appearance of multistable states in the effective classical potential, this effect determines still the behaviors of the temperature-dependent barrier. For a single-well potential, the height of the grown barrier of the ECP increases when the temperature decreases and the damping constant increases. In a double-well potential, the quantum effect depresses the energy barrier, but the nonlocal dissipative action raises the top of the potential barrier. It is concluded that the quantum fluctuation and dissipation play opposite roles in the barrier dynamics. Nonlinear coupling could either lower or raise the ECP barrier compared with the bare potential barrier, thus leading to either hindrance or enhancement of the decay rate, depending on the properties of the coupling form factor. Both cases lead to a nonmonotonic behavior of the temperature-dependent barrier.

ACKNOWLEDGMENTS

This work was supported by the National Natural Science Foundation of China under Grant No. 10075007 and the Foundation of the Ministry of Education, China.

[1] R. P. Feynman and A. R. Hibbs, *Quantum Mechanics and Path Integrals* (McGraw-Hill, New York, 1965).
[2] A. O. Caldeira and A. J. Leggett, Phys. Rev. Lett. **46**, 211 (1981); Physica A **121**, 587 (1983); Ann. Phys. (N.Y.) **149**, 374 (1983).
[3] H. Grabert, P. Olschowski, and U. Weiss, Phys. Rev. B **36**, 1931 (1987).
[4] P. Hänggi, P. Talkner, and M. Borkoves, Rev. Mod. Phys. **62**, 251 (1990).
[5] U. Weiss, *Quantum Dissipative System* (World Scientific, Singapore, 1993).
[6] M. Rosenau da Costa, A. O. Caldeira, S. M. Dutra, and H. Westfahl, Jr., Phys. Rev. A **61**, 022107 (2000).
[7] J. B. Straus, J. M. G. Llorente, and G. A. Voth, J. Chem. Phys. **98**, 4082 (1993); R. Hernandez, *ibid.* **111**, 7701 (1999).
[8] R. Krishan, S. Singh, and G. W. Robinson, Phys. Rev. A **45**, 5408 (1992); J. Chem. Phys. **97**, 5516 (1992).
[9] P. Frobrich and I. I. Gontchar, Phys. Rep. **292**, 132 (1998).
[10] J. Ankerhold, H. Grabert, and G.-L. Ingold, Phys. Rev. E **51**, 4267 (1995).
[11] Sh. Matsumoto and M. Yoshimura, Phys. Rev. A **63**, 012104 (2001).
[12] R. Giachetti and V. Tognetti, Phys. Rev. Lett. **55**, 912 (1985).
[13] R. P. Feynman and H. Kleinert, Phys. Rev. A **34**, 5080 (1986).
[14] H. Kleinert, *Path Integrals in Quantum Mechanics, Statistics and Polymer Physics* (World Scientific, Singapore, 1990).
[15] A. Cuccoli, A. Rossi, V. Tognetti, and R. Vaia, Phys. Rev. E **55**, R4849 (1997).
[16] A. Cuccoli, A. Fubini, V. Tognetti, and R. Vaia, Phys. Rev. E **64**, 066124 (2001).
[17] J. D. Bao, Y. Z. Zhuo, and X. Z. Wu, Phys. Rev. E **52**, 5656 (1995).
[18] J. D. Bao, in *Path Integral from peV to TeV*, edited by V. Tognetti, A. Cuccoli, and R. Vaia (World Scientific, Singapore, 1999), pp. 335–338.
[19] W. H. Miller, S. D. Schwartz, and J. W. Tromp, J. Chem. Phys. **79**, 4889 (1983); J. D. Doll and D. L. Freeman, *ibid.* **80**, 2239 (1984); W. Janke and T. Sauer, Phys. Lett. A **165**, 199 (1992).
[20] J. D. Bao, Y. Abe, and Y. Z. Zhuo, Phys. Rev. E **58**, 2931 (1998).
[21] J. D. Bao, Y. Z. Zhuo, and X. Z. Wu, Z. Phys. A **354**, 239 (1996).
[22] D. E. Makarov and M. Topaler, Phys. Rev. E **52**, 178 (1995).
[23] H. Kleinert, W. Kurzinger, and A. Pelster, J. Phys. A **31**, 8307 (1998).
[24] J. B. Straus and G. A. Voth, J. Chem. Phys. **96**, 5460 (1992).
[25] H. Kleinert, Phys. Lett. A **173**, 332 (1993); H. Kleinert and H. Meyer, *ibid.* **184**, 319 (1994).
[26] M. Bachmann, H. Kleinert, and A. Pelster, Phys. Rev. A **62**, 052509 (2000).
[27] G. R. Haynes and G. A. Voth, Phys. Rev. A **46**, 2143 (1992).